J|A|C|S ARTICLES

Published on Web 03/31/2009

New Paradigm in Molecular Engineering of Sensitizers for Solar Cell Applications

Takeru Bessho,[†] Eiji Yoneda,[†] Jun-Ho Yum,[†] Matteo Guglielmi,[‡] Ivano Tavernelli,[‡] Hachiro Imai,[§] Ursula Rothlisberger,[‡] Mohammad K. Nazeeruddin,*[,†] and Michael Grätzel*[,†]

Laboratory for Photonics and Interfaces, and Laboratory of Computational Chemistry and Biochemistry, Institute of Chemical Sciences and Engineering, School of Basic Sciences, Swiss Federal Institute of Technology, CH - 1015 Lausanne, Switzerland, and Environmental Material Laboratory, Material Science of Engineering, Graduate School of Engineering, Shibaura Institute of Technology, 3-7-5, Toyosu, koutou, Tokyo, Japan

Received January 21, 2009; E-mail: mdkhaja.nazeeruddin@epfl.ch; michael.graetzel@epfl.ch

Abstract: A novel thiocyanate-free cyclometalleted ruthenium sensitizer for solar cells is designed and developed. Upon anchoring to nanocrystalline TiO_2 films, it exhibits a remarkable incident monochromatic photon-to-current conversion efficiency of 83%. The solar cell employing a liquid-based electrolyte exhibits a short circuit photocurrent density of 17 mA/cm^2, an open circuit voltage of 800 mV, and a fill factor of 0.74, corresponding to an overall conversion efficiency of 10.1% at standard AM 1.5 sunlight. To understand the structural, electronic, and optical properties of the cyclometalleted ruthenium sensitizer, we have investigated using density functional theory (DFT) and time-dependent DFT (TDDFT). Our results show the HOMO is located mostly on ruthenium and cyclometalated ligand, while the LUMO is on 4-carboxylic acid-4′-carboxylate-2,2′-bipyridine. Molecular orbitals analysis confirmed the experimental assignment of redox potentials, and TDDFT calculations allowed assignment of the visible absorption bands. The present findings provide new design criteria for the next generation of ruthenium sensitizers and help foster widespread interest in the engineering of new sensitizers that interact effectively with the I^-/I_3^- redox couple.

Introduction

The conversion of sunlight to electricity using dye-sensitized solar cells (DSCs) represents one of the most promising methods for future large-scale power production from renewable energy sources.[1−13] In these cells the sensitizer is one of the key components, harvesting the solar radiation and converting it to electric current. Over the last 17 years, ruthenium complexes endowed with thiocyanate ligands have maintained a clear lead in performance among thousands of dyes that have been scrutinized. Their validated efficiency record under standard air mass 1.5 reporting conditions stands presently at $10.4 \pm 0.3\%$.[14] Many attempts to replace the thiocyanate donor ligands have been made, because the monodentate SCN is believed to be the weakest part of the complex from the chemical stability point of view. However, so far, these efforts have yielded only limited success, as the conversion efficiency achieved with complexes that do not contain SCN remain well below a few percent.[15] Here we report on the novel thiocyanate-free cyclometalated ruthenium complex, which exhibits remarkable performance as a sensitizer. This novel generation of ruthenium complexes

[†] Laboratory for Photonics and Interfaces, Swiss Federal Institute of Technology.

[‡] Laboratory of Computational Chemistry and Biochemistry, Swiss Federal Institute of Technology.

[§] Shibaura Institute of Technology.

(1) O'Regan, B.; Grätzel, M. *Nature (London)* **1991**, *353*, 737–740.
(2) Nazeeruddin, M. K.; Zakeeruddin, S. M.; Humphry-Baker, R.; Jirousek, M.; Liska, P.; Vlachopoulos, N.; Shklover, V.; Fischer, C. H.; Grätzel, M. *Inorg. Chem.* **1999**, *38*, 6298–6305.
(3) Peter, L. M.; Wijayantha, K. G. U. *Electrochim. Acta* **2000**, *45*, 4543–4551.
(4) Hara, K.; Sugihara, H.; Tachibana, Y.; Islam, A.; Yanagida, M.; Sayama, K.; Arakawa, H.; Fujihashi, G.; Horiguchi, T.; Kinoshita, T. *Langmuir* **2001**, *17*, 5992–5999.
(5) Lindstrm̆, H.; Holmberg, A.; Magnusson, E.; Lindquist, S. E.; Malmqvist, L.; Hagfeldt, A. *Nano Lett.* **2001**, *1*, 97–100.
(6) Nazeeruddin, M. K.; Péchy, P.; Renouard, T.; Zakeeruddin, S. M.; Humphry-Baker, R.; Comte, P.; Liska, P.; Cevey, L.; Costa, E.; Shklover, V.; Spiccia, L.; Deacon, G. B.; Bignozzi, C. A.; Grätzel, M. *J. Am. Chem. Soc.* **2001**, *123*, 1613–1624.
(7) Wang, P.; Zakeeruddin, S. M.; Moser, J. E.; Nazeeruddin, M. K.; Sekiguchi, T.; Grätzel, M. *Nat. Mater.* **2003**, *2*, 402–407.
(8) Bisquert, J.; Cahen, D.; Hodes, G.; Ruhle, S.; Zaban, A. *J. Phys. Chem. B* **2004**, *108*, 8106–8118.
(9) Horiuchi, T.; Miura, H.; Sumioka, K.; Uchida, S. *J. Am. Chem. Soc.* **2004**, *126*, 12218–12219.
(10) Park, N. G.; Kang, M. G.; Kim, K. M.; Ryu, K. S.; Chang, S. H.; Kim, D. K.; van de Lagemaat, J.; Benkstein, K. D.; Frank, A. J. *Langmuir* **2004**, *20*, 4246–4253.
(11) Haque, S. A.; Handa, S.; Peter, K.; Palomares, E.; Thelakkat, M.; Durrant, J. R. *Angew. Chem., Int. Ed.* **2005**, *44*, 5740–5744.
(12) Nazeeruddin, M. K.; Wang, Q.; Cevey, L.; Aranyos, V.; Liska, P.; Figgemeier, E.; Klein, C.; Hirata, N.; Koops, S.; Haque, S. A.; Durrant, J. R.; Hagfeldt, A.; Lever, A. B. P.; Grätzel, M. *Inorg. Chem.* **2006**, *45*, 787–797.
(13) Kuang, D.; Walter, P.; Nuesch, F.; Kim, S.; Ko, J.; Comte, P.; Zakeeruddin, S. M.; Nazeeruddin, M. K.; Grätzel, M. *Langmuir* **2007**, *23*, 10906–10909.
(14) Green, M. A.; Emery, K.; Hishikawa, Y.; Warta, W. *Prog. Photovoltaics* **2009**, *17*, 85–94.
(15) Wadman, S. H.; Kroon, J. M.; Bakker, K.; Lutz, M.; Spek, A. L.; van Klink, G. P. M.; van Koten, G. *Chem. Commun.* **2007**, 1907–1909.

 10.1021/ja9002684 CCC: $40.75

presents a promising class of robust and panchromatic sensitizers enabling greatly enhanced DSC performance.

Experimental Section

Analytical Measurements. UV/vis and fluorescence spectra were recorded in a 1 cm path length quartz cell on a Cary 5 spectrophotometer and Spex Fluorolog 112 Spectrofluorimeter, respectively. Electrochemical data were obtained by cyclic-voltammetry using a three-electrode cell and an Auto laboratory System (PGSTAT 30, GPES 4.8 software). The working electrode was a 0.03 cm^2 glassy carbon disk, the auxiliary electrode was a platinum plate, and a platinum wire was used as quasi-reference electrode. The sensitizers were dissolved in dimethylformamide (DMF) containing 0.1 M tetrabutylammonium hexafluorophosphate as the supporting electrolyte. After the measurement, ferrocene was added as the internal reference for calibration. ^{1}H and ^{13}C NMR spectra were measured on a Bruker 200 MHz spectrometer. The reported chemical shifts were in PPM against TMS.

Synthesis of 2-(2,4-Difluorophenyl)pyridine. A mixture of 2-bromopyridine (1.89 g, 12.0 mmol), 2,4-difluorophenylboronic acid (2.30 g, 14.5 mmol), and K_2CO_3 (6 g, 43.5 mmol) in toluene (60 mL) and water (10 mL) were degassed with Ar for 15 min. $Pd(PPh_3)_4$ (800 mg, 0.66 mmol) was added, and the resulting mixture was heated to 90 °C for 48 h under Ar. After being cooled to room temperature, the aqueous phase was separated and extracted with EtOAc (3 × 100 mL). The combined organic fractions were washed with brine, dried over $MgSO_4$, filtered, and evaporated. The crude compound was purified by column chromatography (SiO_2, $CHCl_3$/hexane, 50/50 then $CHCl_3$) to afford 1.65 g (72%) of the titled compound as a colorless oil which solidify upon standing.

^{1}H NMR (ppm in CD_3OD with NaOD, 400 MHz): 8.72 (d, J = 6.0 Hz, 1H), 8.02 (t, J = 7.1 Hz, 1H), 8.00 (t, J = 7.2 Hz, 1H), 7.78 (d, J = 6.1 Hz, 1H), 7.25 (d, J = 6.0 Hz, 1H), 7.02 (t, J = 7.1 Hz, 1H), 6.92 (t, J = 7.2 Hz, 1H).

Synthesis of Bis(4,4′-dicarboxy-2,2′-bipyridine) 2-(2,4-Difluorophenyl)pyridine Ruthenium (II). *cis*-Dichloro-bis(4,4′-dicarboxy-2,2′-bipyridine)ruthenium (0.50 g, 0.757 mmol) and 2-(2,4-difluorophenyl)pyridine (0.279 g 1.51 mmol) were dissolved in ethylene glycol (75 mL), and the reaction mixture was heated to 170 °C under Ar for 2 h. Then tetra-butyl ammonium hydroxide (3.02 g, 3.77 mmol) was added to the reaction mixture and further heated to 170 °C under Ar for 2 h. After evaporating the solvent, the resulting solid was dissolved in H_2O (20 mL) and was titrated with 0.2 M HNO_3 to pH 3.80. The reaction mixture was kept in a refrigerator overnight, and allowed to warm to 25 °C. The resulting precipitation was collected on a sintered glass crucible by suction filtration. The solid was dissolved in a basic H_2O solution (pH 10−11) and purified on a Sephadex LH-20 column by eluting with H_2O. Yield, 170 mg. ^{1}H NMR (ppm in CD_3OD with NaOD, 400 MHz): 9.08 (s, 1H), 9.01 (s, 1H), 8.95 (s, 2H), 8.32 (d, J = 7.5 Hz, 1H), 8.17 (d, J = 7.3 Hz, 1H), 7.90 (m, 5H), 7.77 (m, 4H), 7.58 (d, J = 7.2 Hz, 1H), 7.02 (td, J = 2.3 and 7.2 Hz, 1H), 6.42 (td, J = 2.5 and 9.3 Hz, 1H), 5.85 (dd, 2.3 and 7.0 Hz, 1H), 3.25 (q, J = 7.5 Hz, 8H), 1.65 (m, 8H), 1.40 (m, 8H), 1.00 (t, J = 7.6 Hz, 12H). ^{13}C NMR (ppm in CD3OD, 100 MHz): 198, 168, 163, 161, 160, 159, 157, 156, 156, 154, 153, 152, 150, 149, 148, 147, 145, 145, 144, 143, 142, 136, 127, 126, 125, 124, 124, 123, 122, 122, 122, 121, 121, 120, 115, 57, 22, 18, 11.

Solar-Cell Fabrication and Characterization. The photoanode is a square type (4 × 4 mm) TiO_2 electrode, containing a 12 μm thick film of 20 nm sized particles on which a 5 μm thick layer of 400 nm sized scattering particles was superimposed. The prepared TiO_2 electrodes[6] were heated at 450 °C for 20 min under an O_2 atmosphere and allowed to cool under 100 °C before dipping into the dye solution. The complex **1** dye solutions were prepared in ethanol with typical concentrations in the range of $2-5 \times 10^{-4}$ M, and the electrodes were left in the dye solutions for 18−20 h. A sandwich cell was prepared by using the dye anchored TiO_2 film as a working electrode and a counter electrode, which was coated with platinum. The two electrodes were superimposed with a thin transparent film of Surlyn polymer gasket (DuPont), and the superimposed electrodes were tightly held and applied heat (130 °C) around the Surlyn gasket to seal the two electrodes. A thin layer of electrolyte solution containing 0.60 M butylmethylimidazolium iodide (BMII), 0.03 M I_2, 0.10 M guanidinium thiocyanate, and 0.50 M *tert*-butylpyridine in a mixture of acetonitrile and valeronitrile volume ratio, 85:15 (A6141), was introduced into interelectrode space from the counterelectrode side through a predrilled hole. Then, the drilled hole was sealed with microscope cover slide and Surlyn to avoid leakage of the electrolyte solution. On the photoanode, an antireflection layer ((λ < 380 nm, ARKTOP, MIHAMA, Japan) was attached. For photovoltaic measurements of the DSCs, the irradiation source was a 450 W xenon light source (Osram XBO 450, U.S.A.), whose power of an AM 1.5 solar simulator was calibrated by using a reference Si photodiode equipped with an IR cutoff filter (KG-3, Schott) to reduce the mismatch in the region of 350−750 nm between the simulated light and AM 1.5 to less than 2%. The measurement delay time of photo I−V characteristics of DSCs was fixed to 0.1 V s^{-1}. The measurement of incident photon-to-current conversion efficiency (IPCE) was plotted as a function of excitation wavelength by using the incident light from a 300 W xenon lamp (ILC Technology, U.S.A.), which was focused through a Gemini-180 double monochromator (Jobin Yvon Ltd.). The active area of TiO_2 electrodes was measured precisely by using a scanner, and a light shading mask was used on the photoanode to reduce scattered light from the edge of the glass electrodes of the dyed TiO_2 layer.[16]

Computational Details. Calculations were performed using the software package TURBOMOLE[17] with the basis set def2-TZVP[18] for all atoms. The exchange and correlation energy was estimated using the functional B3LYP.[19] Solvation effects were included using the implicit solvent model COSMO[20] with a dielectric constant for dimethylformamide (DMF) at 38.25. For the ruthenium atom we used the quasirelativistic Stuttgart/Dresden semicore SDD-ECP.[21] Open-shell electronic configurations were computed using unrestricted density functional theory (DFT). All configurations were converged to a maximum electronic gradient of 10^{-7} atomic units. The vertical singlet to singlet transitions were calculated with time-dependent DFT (TDDFT)/COSMO[22,23] using the same basis sets and exchange-correlation functional as for the ground-state calculations. All values given in the text refer to the neutral compounds, which are the most likely protomers at the chosen experimental conditions. Test calculations were also performed for other protonation states (4H and 2H) with only minor effects on the electronic properties (results given in the Supporting Information).

Results and Discussion

Scheme 1 shows the synthetic approach used to obtain cyclometalated ruthenium sensitizer bis(4,4′-dicarboxy-2,2′-bipyridine) 2-(2,4-difluorophenyl)pyridine ruthenium(II), which hereafter is referred to as complex **1**.

(16) Ito, S.; Nazeeruddin, M. K.; Liska, P.; Comte, P.; Charvet, R.; Pechy, P.; Jirousek, M.; Kay, A.; Zakeeruddin, S. M.; Grätzel, M. *Prog. Photovoltaics* **2006**, *14*, 589–601.
(17) Bauernschmitt, R.; Ahlrichs, R. *Chem. Phys. Lett.* **1996**, *256*, 454–464.
(18) Weigend, F.; Ahlrichs, R. *Phys. Chem. Chem. Phys.* **2005**, *7*, 3297–3305.
(19) Becke, A. D. *J. Chem. Phys.* **1993**, *98*, 5648–5652.
(20) Klamt, A.; Schüürmann, G. *J. Chem. Soc.* **1993**, 799–805.
(21) Andrae, D.; Haussermann, U.; Dolg, M.; Stoll, H.; Preuss, H. *Theor. Chim. Acta* **1990**, *77*, 123–141.
(22) Furche, F.; Ahlrichs, R. *J. Chem. Phys.* **2002**, *117*, 7433–7447.
(23) Furche, F.; Rappoport, D. *Density functional theory for excited states: equilibrium structure and electronic spectra. Ch. III of Computational Photochemistry*; Elsevier: Amsterdam, 2005; Vol. 16.

Scheme 1. Synthetic Route for Bis(4,4′-dicarboxy-2,2′-bipyridine) 2-(2,4-Difluorophenyl)pyridine Ruthenium(II)

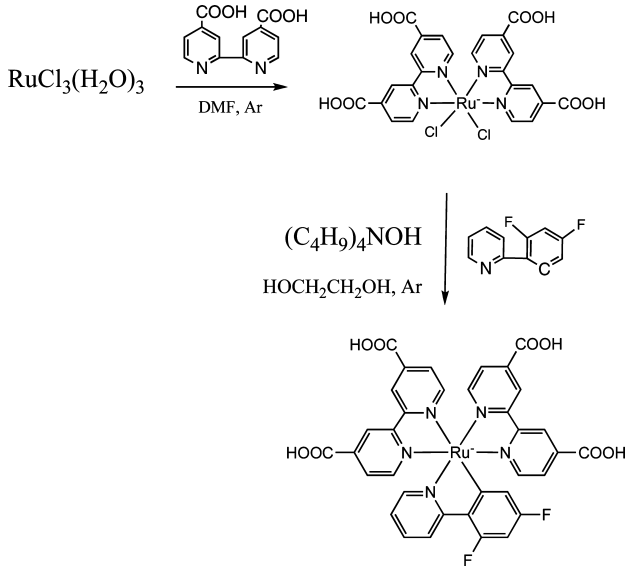

The absorption spectrum of complex **1** (Figure 1) is dominated in the visible region by three bands at 406, 490, and 560 nm, which are attributed to metal-to-ligand (MLCT) charge transfer transitions. The lowest energy MLCT band in complex **1** is red-shifted by 25 nm when compared to the standard bis-tetrabutylammonium *cis*-dithiocyanatobis-2,2′-bipyridine-4-COOH,4′-COO^--ruthenium(II) (N719) sensitizer (Figure 1). The striking feature of complex **1** is the presence of a new band at 490 nm, with high molar extinction coefficient compared to the standard N719 sensitizer whose spectrum shows a valley in this wavelength domain (see Figure S1 in Supporting Information).

To gain further insight into the electronic properties of this important new class of sensitizers, we have performed theoretical calculations using both DFT for the ground-state geometries and TDDFT for the excited-state energies and properties (see Computational Details). The computed spectrum in the visible region is in very good agreement with the experimental one (Figure 1).

Table 1. Character Table of Calculated Vertical Excitations 1, 2, and 3 (Black Bars in Figure 1) for Complex **1**[a]

	characters		
elec. transitions	occupied orbitals	empty orbitals	contributions (%)
1	H-2	L+1	39.2
	H-2	L	23.0
	H-1	L+1	17.1
2	H	L+2	54.4
	H-1	L+1	33.3
3	H-2	L+2	53.8
	H	L+4	31.9

[a] Contributions below 5% are not shown.

The nature of the three main bands in this energy range can be characterized by the difference between the corresponding ground state and excited states electron density distributions. We find that the first band (Table 1) is mainly characterized by a pure metal to ligand charge transfer with the main component of the transferred density on the pyridine moiety trans to the nitrogen atom of the difluorophenyl−pyridine ligand. The second and third bands show a sizable delocalization of the hole onto the carbanionic group, an effect that is particularly strong for the new band around 490 nm (Table 1). In contrast to the first band, the excited electron density for the second and third bands is now mainly localized on the bipyridine ligand trans to the cyclometalated moiety.

The relevant occupied and unoccupied Kohn−Sham molecular orbitals of complex **1** involved in the transitions are shown in Figure 2 and their contributions to the main electronic transitions are listed in Table 1.

The cyclic voltammogram of the complex **1** exhibits a quasi-reversible metal centered oxidation at $E_{1/2} = 1.08$ V versus NHE, assigned to the $Ru^{III/II}$ couple. Under similar conditions the N719 complex shows an oxidation wave at 1.12 V versus NHE. When scanning toward negative potentials one quasireversible wave at $E_{1/2} = -1.20$ NHE was observed, which is assigned to the reduction of the 4,4′-dicarboxylic acid ligand. In full accord

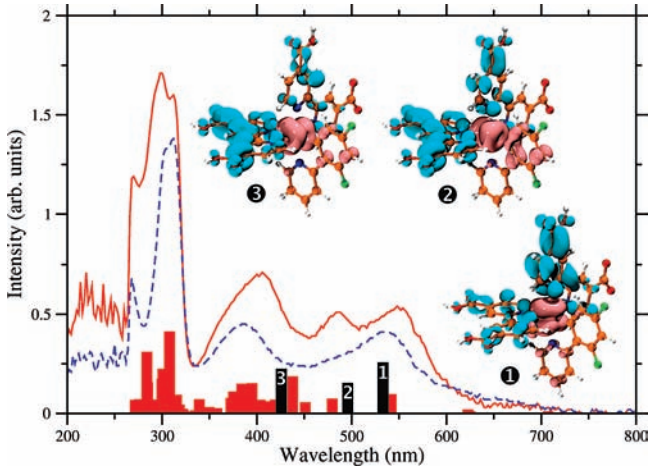

Figure 1. UV−vis experimental absorption spectra of complex **1** (red line) and N719 (dashed blue line) measured in DMF solution. Red bars represent the computed vertical electronic excitations intensities (TDDFT) of complex **1**. For three selected optically active electronic transitions (black bars with labels 1, 2, and 3 at 533, 496, and 426 nm, respectively) the electron−hole density plots are shown (hole and excited electron densities are represented in pink and cyan, respectively).

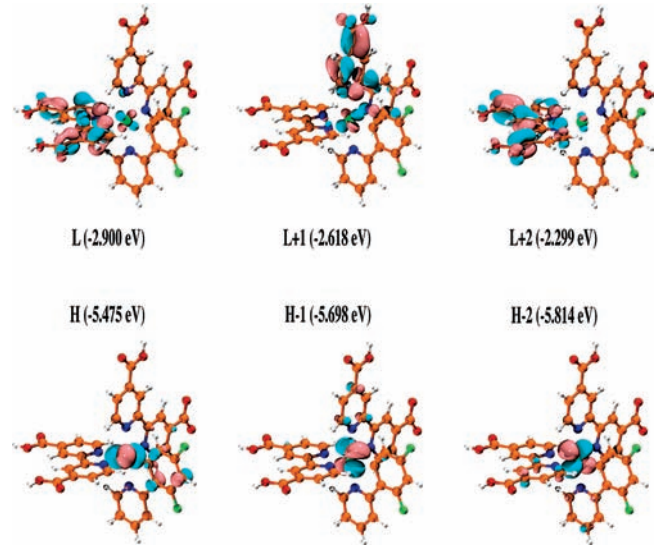

Figure 2. Computed isosurface plots of selected Kohn−Sham molecular orbitals (from HOMO-2 to LUMO+2) of complex **1**, which are mainly involved in the optically active electronic transitions 1, 2, and 3 (black bars in Figure 1).

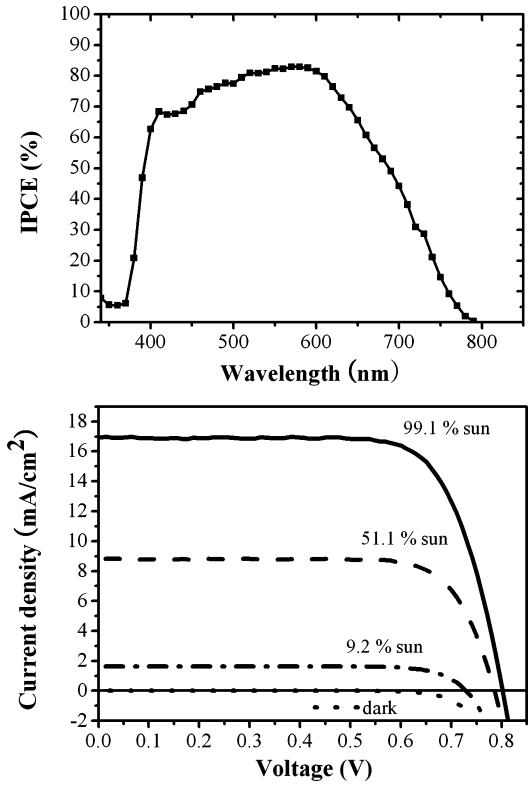

Figure 3. Incident photon to current conversion efficiency (top panel) and photocurrent−voltage curve (bottom panel) of a DSC, employing complex **1** measured under different light intensity, with the spectral distribution matching the standard AM 1.5 solar radiation: 99.1 mW cm^{-2} (solid line), 51.1 mW cm^{-2} (dashed line), and 9.2 mW cm^{-2} (dash-dotted line). The cell is masked with black plastic to avoid optical artifacts, with the aperture area being 0.152 cm^2.

with experiments, the DFT calculations predict an ionization potential (IP) difference between the two compounds of ~0.04 V, an agreement that might partially be due to a fortuitous cancelation of errors. The excited-state oxidation potential of a sensitizer plays an important role in the electron transfer process, for which an approximate value can be extracted from the ground-state oxidation couple and the zero−zero excitation energy $E^{(0-0)}$ according to eq 1.

$$E(S^+/S^*) = E(S^+/S) - E^{(0-0)} \quad (1)$$

The $E^{(0-0)}$ energy (1.84 eV) was derived from the high energy side of the corrected emission spectra where the intensity is 10% of the peak intensity. The calculated excited-state oxidation potential of the sensitizer complex **1** is −0.76 V versus NHE, which is notably more negative than the TiO_2 conduction band for injecting electrons efficiently. On the other hand, the oxidation potential of the complex **1** is 0.5 V more positive than the I^-/I_3^- redox couple, providing ample driving force for regeneration of the dye.

Figure 3 shows the photovoltaic performance of a solar cell employing a screen printed nanocrystalline TiO_2 film. The incident monochromatic photon-to-current conversion efficiency (IPCE) plotted as a function of excitation wavelength shows a plateau between 500−600 nm reaching 83% at 570 nm. From the overlap integral of this curve with the AM 1.5 spectral solar photon flux one derives a short circuit photocurrent density of 17.1 mA cm^{-2}. In agreement with this prediction, complex **1** sensitized cell gave under standard global AM 1.5 solar conditions a short circuit photocurrent density (i_{sc}) of 17 ± 0.1 mA cm^{-2}, indicating negligible spectral mismatch between the solar light and the simulator employed. The open circuit voltage (V_{oc}) was 800 ± 5 mV and the fill factor (ff) was 0.74 ± 0.02. Using these values, one derives an overall efficiency, $\eta = i_{sc} \times V_{oc} \times$ ff, of 10.1 ± 0.1%.

The 10% efficiency achieved by the cyclometalated complex **1** sensitized TiO_2 solar cell device can be related to the dye's broad range of visible light absorption caused by the cyclometalated ligand, whose electron donating property is modulated by the presence of the two fluorine substituents. The role of the fluorine is to reduce the Lewis basicity of the carbanion in the cyclometalated ligand, possibly adjusting the Ru(II)/Ru(III) redox potential at a level where rapid regeneration of the sensitizer by the iodide ion is possible. The presence of the carbanionic ligand stabilizes the Ru(III) state that is generated upon oxidation of the complex during injection of an electron into the conduction band of the TiO_2. The positive charge is shared by the cyclometalated ligand allowing rapid transfer to the iodide ions in the adjacent electrolyte. The importance of the role of the fluorine substituents in tuning the electron donating property of the ligand is confirmed by the observation that a sensitizer containing no fluorine on the cyclometalated ligand is less efficient than complex **1**.

The difference in ionization potentials ($\Delta IP = IP_{(complex\ 1)} - IP_{(complex\ 2)}$) for the fluorine- and the hydrogen-substituted compounds was computed to be 0.17 eV. The computed data are in excellent corroboration with experimentally measured oxidation potentials of complex **1** and its analogous complex without fluorine on the cyclometalated ligand.

The presence of carboxylic groups allows stable anchoring of the sensitizer to the semiconductor surface, so as to ensure a high electronic coupling between the dye and the semiconductor, which is required for efficient charge injection. The DFT calculations clearly show that the optically active electronic excitations in the visible are made of transitions from the three highest HOMOs, which lie within ~0.35 eV and have a strong ruthenium t_{2g} character. The new band at 490 nm is characterized by a transition from the HOMO, which has a sizable π-orbital contribution from the cyclometalated ligand (see Table 1 and Figure 2). The LUMOs involved in the former excitations are a set of π^*-orbitals localized on the bipyridines ligands bearing the protonated carboxylic groups (see Table 1 and Figure 2). These orbitals will give rise to strongly mixed dye-TiO_2 states upon absorption on the TiO_2 nanoparticles. Therefore, the excited states generating the absorption spectrum might strongly couple to the TiO_2 conduction band states, eventually leading to efficient electron injection and increased photocurrents.

Conclusions

In conclusion, the present study establishes that judicious molecular engineering of cyclometalated ruthenium complexes, in particular, the introduction of two fluorine atoms in the phenyl ring of the phenylpyridine ligand, leads to a highly efficient charge transfer sensitizer. Application of TDDFT calculation has provided valuable information on the nature of the electronic transitions that are involved in the light absorption and electron transfer process. This method

will provide critical clues on the synthetic choice of structural modifications that will boost further their light harvesting and charge generating ability. This new generation of ruthenium complexes shows great promise to become a leading class of robust and panchromatic sensitizers, enabling greatly enhanced DSC performance.

Acknowledgment. We acknowledge financial support of this work by the Swiss Federal Office for Energy (OFEN). We thank Dr. Robin Humphry-Baker, S. M. Zakeeruddin, Peter Péchy, Pascal Comte, and Paul Liska for their kind assistance. A note of thanks goes to Christian Clémençon and Pascal Jermini (BG/L System Administrators at the EPFL) for their technical support.

Supporting Information Available: Table reporting the Kohn−Sham frontier orbital energies and ionization potentials for different protonation states of complex **1**, complex **2**, and N719. This material is available free of charge via the Internet at http://pubs.acs.org.

JA9002684